Chinese Chemical Letters 33 (2022) 314–319

Contents lists available at ScienceDirect

Chinese Chemical Letters

journal homepage: www.elsevier.com/locate/cclet

Aqueous-phase synthesis of upconversion metal-organic frameworks for ATP-responsive *in situ* imaging and targeted combinational cancer therapy

Lin Yang[a], Shuaidong Zhu[a], Zhimei He[a], Xiangli Li[a], Jiangning Chen[a], Sai Bi[b,*], Jun-Jie Zhu[a,*]

[a] *State Key Laboratory of Analytical Chemistry for Life Science, School of Chemistry and Chemical Engineering, School of Life Sciences, Nanjing University, Nanjing 210023, China*
[b] *College of Chemistry and Chemical Engineering, Qingdao University, Qingdao 266071, China*

ARTICLE INFO

Article history:
Received 15 May 2021
Revised 1 July 2021
Accepted 2 July 2021
Available online 11 July 2021

Keywords:
Upconversion nanoparticles
Metal-organic frameworks
ATP response
In situ imaging
Targeted combinational therapy

ABSTRACT

Herein, the nanoscaled ATP-responsive upconversion metal-organic frameworks (UCMOFs) are aqueous-phase synthesized for co-delivery of therapeutic protein cytochrome c (Cyt c) and chemodrugs doxorubicin (DOX), achieving targeted combinational therapy of human cervical cancer. The UCMOFs are rationally fabricated by growing ZIF-90 on mesoporous silica-coated upconversion nanoparticles (UCNPs), in which the ZIF-90 layer attenuates the upconversion luminescence (UCL) and the rigid frameworks increase the stability of encapsulated proteins. Once the UCMOF@DOX/Cyt c are internalized into HeLa cells *via* specific recognition of sgc8 aptamers, the intracellular ATP triggers the dissolution of ZIF-90 into Zn^{2+}, which facilitates not only the release of Cyt c and DOX but also the restoration of UCL for real-time monitoring of drug release. It has been demonstrated that the therapeutic efficacy is greatly improved by the combination of caspase-mediated apoptosis activated by Cyt c (protein therapeutics), DNA fragmentation induced by DOX (chemotherapy), and Zn^{2+}-promoted generation of reactive oxygen species (ROS) (oxidative stress). Overall, our proposed multifunctional UCMOFs provide an effective platform for targeted combinational cancer therapy and *in situ* imaging, which hold great promise in biomedical and clinical applications.

Combinational cancer therapy, in which two or more agents are used to inhibit tumor growth, has drawn tremendous attention in recent years due to its enhanced therapeutic efficacy for cancer cells [1]. Chemotherapy is one of the principal modalities in clinical cancer treatments, which however often suffers from the systematic toxicity due to the uptake of drugs by the reticuloendothelial system [2]. Notably, protein therapeutics with high specificity, great activity and low toxicity has become an attractive approach for cancer therapy [3,4]. Nevertheless, the protein curative efficacy is usually hampered by the poor cell membrane permeability and inhospitable denaturation conditions. Thus, the development of desirable nanovehicles that enable the effective co-delivery of chemodrugs and therapeutic proteins for combinational therapy and preserve the biological activity of proteins is in an urgent need.

Recently, various nanocarriers have been established for drug delivery applications [5,6]. However, these nanoplatforms are often challenged by poor stability, nonspecific leakage of drugs during transportation, aggregation and denaturation of protein agents, and so on [7]. Alternatively, metal-organic frameworks (MOFs) have emerged as a powerful kind of porous materials for multi-drugs transport [8,9]. The drug molecules are confined in the pores of MOFs, which thus significantly increases the encapsulation stability [10-12]. In particular, zeolitic imidazolate frameworks (ZIFs) have become the most widely explored MOFs for biomedical applications, which can be synthesized under biologically compatible conditions and readily respond to various cellular microenviroment (*e.g.* ATP and acidic condition) [13,14].

Moreover, the development of multifunctional nanoplatforms by integrating multimodal therapy with *in situ* imaging is of particular interest for tracking the location of nanocarriers and monitoring the release of drugs in cancer therapy with high spatiotemporal resolution. Upconversion nanoparticles (UCNPs), a kind of optical nanotransducers which can convert near-infrared (NIR) light to

* Corresponding author.
E-mail addresses: bisai11@126.com (S. Bi), jjzhu@nju.edu.cn (J.-J. Zhu).

https://doi.org/10.1016/j.cclet.2021.07.007
1001-8417/

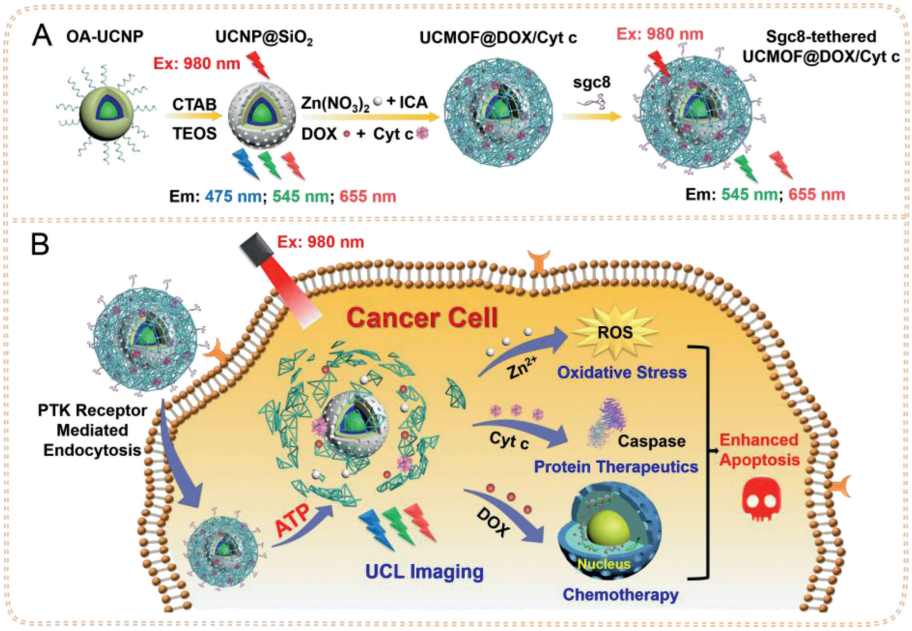

Fig. 1. Schematics of ATP-responsive UCMOFs for *in situ* imaging and targeted combinational cancer therapy.

UV and/or visible light, have been versatilely applied in bioassay and bioimaging, drug delivery systems, and photodynamic therapy due to their deep tissue penetration, low background autofluorescence, high resistance to photobleaching and narrow emission bandwidths [15,16]. Currently, the upconversion metal-organic frameworks (UCMOFs) have attracted the interest of researchers in NIR luminescence imaging and cancer treatment [17,18]. However, the encapsulation of protein molecules into UCMOFs for protein therapeutics is still limited by the rigid synthesis conditions of UCMOFs, such as high temperature or organic solvents, which can influence the structure and bioactivity of proteins. Thus, the aqueous-phase preparation of UCMOFs is essential to develop the multifunctional nanocarriers for biomolecules delivery.

Herein, an aqueous-phase synthesis approach has been developed to fabricate UCMOFs for the cytosolic co-delivery of therapeutic protein and chemodrugs, achieving targeted combinational therapy of cervical cancer and real-time monitoring of drug release (Fig. 1). Due to the overlapping absorption of organic links 2-imidazolate carboxaldehyde (ICA) of ZIF-90 with UCL emission, the luminescence of UCNPs are effectively quenched by the MOF shell. In this study, a model protein drug Cyt c and small-molecule chemotherapeutic agent DOX are co-encapsulated in ZIF-90 shell *via* a *de novo* approach for combinational therapy. To endow the nanovehicles with targeting capability, the sgc8 aptamers are assembled on the surface of UCMOFs, which can specifically recognize the overexpressed protein tyrosine kinase 7 of cervical cancer cells [19]. After internalized into the target cells (*e.g.* HeLa cells) *via* receptor-mediated endocytosis, the UCMOFs are degraded by ATP in the cytosol [9], resulting in the restoration of UCL to monitor the release of the encapsulated drugs (Cyt c and DOX) and metal ions (Zn^{2+}). Here, Cyt c can initiate the mitochondrial apoptosis pathway and result in the programmed cell death *via* caspase-mediated apoptosis [20], while DOX is able to induce the DNA fragmentation in nucleus and inhibit tumor growth [21]. In addition, the Zn^{2+}-mediated generation of reactive oxygen species (ROS) can cause the oxidative damage to the cancer cells and further improve the therapeutic efficacy.

The prepared UCMOFs are first characterized. In this study, a modified thermal decomposition method was used to prepare the oleic acid (OA) coated core-shell-shell UCNP $NaYF_4$:Yb,Er@$NaYF_4$:Yb,Tm@$NaYF_4$ (OA-UCNP) [22]. The TEM images show that the size of $NaYF_4$:Yb,Er core is 16 ± 2 nm (Fig. 2A), which increases to 23 ± 2 nm when coated with the inner shell $NaYF_4$:Yb,Tm (Fig. 2B), and then up to 29 ± 3 nm in length after coated with the outer shell $NaYF_4$ (Fig. 2C). The high-resolution TEM (HRTEM) demonstrates that the *d*-spacing between the two adjacent lattice planes is 0.52 nm, attributing to the (100) plane of β-phase UCNPs (inset of Fig. 2C). To promote the growth of ZIF-90 on UCNPs in aqueous phase, a mesoporous silica coating strategy was adopted to convert the hydrophobic OA-UCNP into hydrophilic UCNP@SiO_2. Fig. 2D shows that UCNP@SiO_2 with the silica shell thickness of ~9 nm can be well mono-dispersed in water. Small-angle X-ray diffraction result confirms that UCNP@SiO_2 has the standard MCM-41 structure attributed to mesopores of SiO_2 layer (Fig. S1 in Supporting information).

Subsequently, ZIF-90 with good hydrophilicity is self-assembled on UCNP@SiO_2 to form the core-shell UCMOFs [14]. Fig. 2E shows the uniform and spherical core-shell UCMOF nanostructures with the MOF shell thickness of 14 ± 3 nm. It should be noted that the MOF shell thickness of UCMOFs can be well controlled by changing the ratio of the MOF precursors to UCNP@SiO_2. The MOF shell thickness of UCMOFs can be controlled from ~9 nm to ~28 nm by changing the ratio of the MOF precursors to UCNP@SiO_2 from 1:1 to 3:1 (Fig. S2 in Supporting information). In addition, the crystal structure of UCMOFs is corresponding to the pure hexagonal phase of $NaYF_4$ and ZIF-90 (Fig. 2I).

Herein, Cyt c and DOX are co-encapsulated into UCMOFs *via* a *de novo* approach, in which MOFs are grown in the presence of proteins and the proteins are embedded in MOFs with small pores, rather than located in large pores [11,12,14]. The TEM image exhibits the uniform and mono-dispersed morphology of the resultant UCMOF@DOX/Cyt c with the size of 67 ± 6 nm (Fig. 2F), and the composition is verified by elemental mapping images (Fig. 2L). As expected, the elements Y and Si are distributed in the UCNP@SiO_2 core, while the element Zn are mainly present in ZIF-90 shell and S represented Cyt c are homogenously distributed in the whole nanostructures, suggesting the successful encapsulation of Cyt c into UCMOFs. The presence of Cyt c in UCMOFs is further characterized by FT-IR (Fig. S3 in Supporting information). Further, the polyvinylpyrrolidone-surface-adsorbent exchange con-

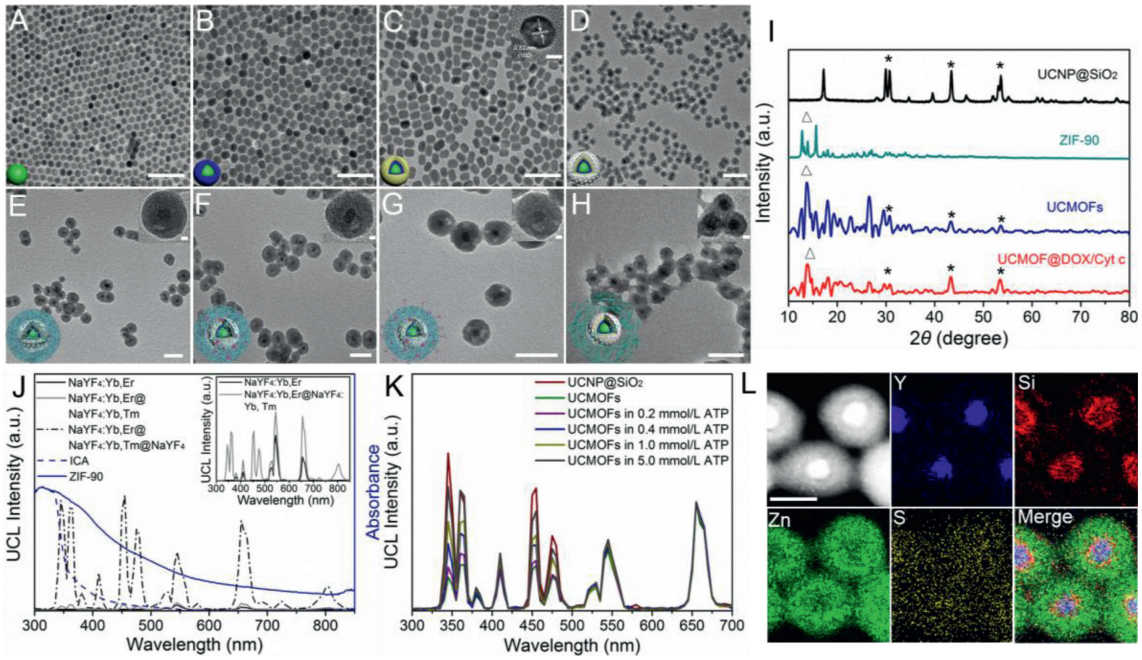

Fig. 2. TEM images of (A) $NaYF_4$:Yb,Er, (B) $NaYF_4$:Yb,Er@$NaYF_4$:Yb,Tm, (C) $NaYF_4$:Yb,Er@$NaYF_4$:Yb,Tm@$NaYF_4$ in cyclohexane (inset of C: the HRTEM image of UCNPs), (D) UCNP@SiO_2, (E) UCNP@SiO_2@ZIF-90 (UCMOFs), (F) UCMOF@DOX/Cyt c, (G) sgc8-tethered UCMOF@DOX/Cyt c in water, and (H) in 5 mmol/L ATP. Insets of E-H: High-magnification TEM images of corresponding nanocomposites. (I) PXRD of UCNP@SiO_2, ZIF-90, UCMOFs and UCMOF@DOX/Cyt c. (J) UCL emission spectra of $NaYF_4$:Yb,Er, $NaYF_4$:Yb,Er@$NaYF_4$:Yb,Tm and $NaYF_4$:Yb,Er@$NaYF_4$:Yb,Tm@$NaYF_4$, and UV-vis absorption spectra of ICA and ZIF-90. Inset of J: Enlarged UCL emission spectra of $NaYF_4$:Yb,Er and $NaYF_4$:Yb,Er@$NaYF_4$:Yb,Tm. (K) UCL emission spectra of UCMOFs treated with different concentrations of ATP. (L) High-angle annular dark-field scanning TEM (HAADF-STEM) and element mapping images of UCMOF@DOX/Cyt c. Scale bars in A-H: 100 nm. Scale bars in L and insets of C and E-H: 10 nm.

firms that Cyt c are mostly embedded in the ZIF-90 shell, rather than just adsorbed onto the surface of ZIF-90 (Fig. S4 in Supporting information). The encapsulation efficiency of Cyt c in ZIF-90 shell is calculated to be ~60 mg/g by thermogravimetric analysis (TGA) (Fig. S5A in Supporting information). In addition, the powder X-ray diffraction (PXRD) pattern shows that the crystalline structure of UCMOF@DOX/Cyt c agrees well with UCMOFs, indicating the little influence of incorporated therapeutic agents on ZIF-90 (Fig. 2I). Meanwhile, the maximum DOX loading capacity in UCMOFs is calculated to be 356 mg/g by monitoring the UV-vis change of DOX at 490 nm before and after encapsulation in supernatant (Fig. S6 in Supporting information). After tethering sgc8 aptamers on ZIF-90 *via* electrostatic adsorption, no significant morphology change is observed (Fig. 2G), and the increased hydrodynamic diameter verifies the formation of sgc8-tethered UCMOFs (Fig. S7A in Supporting information). In addition, the zeta potential turns to the negative potential (−13.3 mV) after attaching aptamers due to the negative charge of nucleic acids (Fig. S7B in Supporting information). The simultaneous loading of DOX and Cyt c and attachment of sgc8 aptamers on UCMOFs are further confirmed by UV-vis spectra (Fig. S7C in Supporting information). The coating density of sgc8 aptamers on UCMOFs is calculated to be 3.6 nmol/mg (Fig. S8 in Supporting information). Benefiting from the conjugation with aptamers, the UCMOFs can be well dispersed in not only saline solution but also cell culture medium even after 24 h of incubation (Fig. S9 in Supporting information), indicating the good stability of the fabricated sgc8-tethered UCMOFs in physiological environment.

By virtue of the competitive coordination between Zn^{2+} and ATP, the ZIF-90 shell can be disintegrated in the presence of ATP, resulting in the simultaneous release of Cyt c and DOX. A quite complete disintegration of ZIF-90 shell is observed after treated with 5 mmol/L ATP (Fig. 2H). The release profiles of Cyt c and DOX in response to different concentrations of ATP display an increased release rate with increasing the concentration of ATP (Figs. S5B and S6C in Supporting information). When the UCMOF@DOX/Cyt c are incubated with 0.4 mmol/L ATP (extracellular level of ATP), a slow release rate of Cyt c (25%) and DOX (10%) is observed even after 24 h. In contrast, after incubated with 5 mmol/L ATP for 0.5 h, the release rates of Cyt c and DOX are ~30%, which reach to more than 60% at 4 h. Thus, the decomposition of ZIF-90 is dependent on the concentration of ATP. In addition, when the nanocomposites are incubated with cell culture medium, nearly no release of Cyt c and DOX is observed (Fig. S10 in Supporting information). These results indicate that the fabricated UCMOFs can remain intact in extracellular environment (the concentration of ATP is below 0.4 mmol/L) to preclude drug release, while the intracellular environment (the concentration of ATP is 1—10 mmol/L) can facilitate the effective release of drugs, which thus can avoid the drug leakage during the transportation and reduce the side effect to normal tissues.

Due to the overlap of ICA absorption spectrum with the UCL emission band centered at 345, 360, 455 and 475 nm, which are assigned to the $^1I_6 \rightarrow {}^3F_4$, $^1D_2 \rightarrow {}^3H_6$, $^1D_2 \rightarrow {}^3F_4$ and $^1G_4 \rightarrow {}^3H_6$ transitions of Tm^{3+} respectively, up to 60% of the emission bands can be effectively quenched by the ZIF-90 shell (Figs. 2J and K). As increasing the ATP concentration from 0.2 mmol/L to 5 mmol/L, the emission intensity of UCMOFs is increased accordingly due to the decomposition of ZIF-90 shell (Fig. 2K). Therefore, the switchable UCL can be applied to monitor the decomposition of ZIF-90 and the release of therapeutic agents.

To determine the protection provided by UCMOFs for protein, the enzymatic activity of Cyt c is investigated upon encapsulation into and release from the UCMOFs, as well as exposure to proteolytic agents and elevated temperature (Fig. S11 in Supporting information). Firstly, the peroxidase activity of free Cyt c is examined and considered as 100% by a standard method, in which ABTS is used as the substrate [10]. Compared with free Cyt c, the encapsulated Cyt c in ZIF-90 shows a slightly increased activity (115%), owing to the interaction between Zn^{2+} in the ZIF-90 and the embedded Cyt c [10]. Upon treated with 5 mmol/L ATP, the activity of Cyt c released from UCMOFs remains 98%, suggesting that the

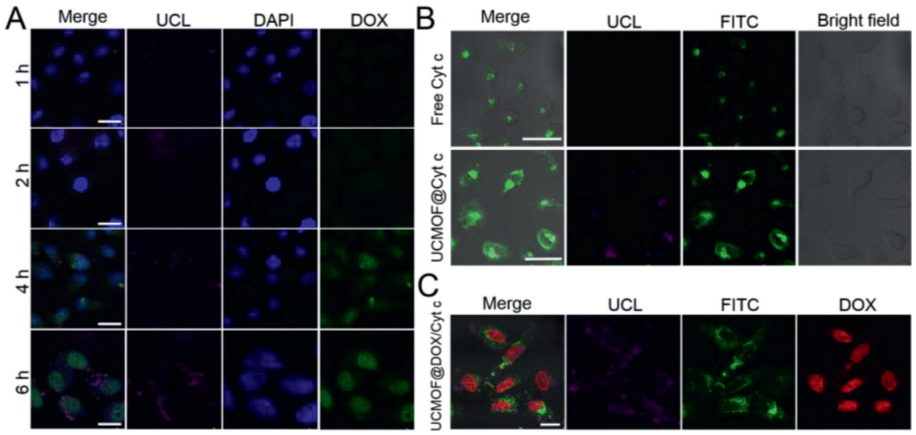

Fig. 3. (A) CLSM images of HeLa cells incubated with sgc8-tethered UCMOF@DOX for different time durations. Scale bar: 25 μm. (B) CLSM images of HeLa cells incubated with free Cyt c and sgc8-tethered UCMOF@Cyt c (Cyt c labeled with FITC) for 6 h. Scale bar: 50 μm. (C) CLSM images of HeLa cells incubated with UCMOF@DOX/Cyt c for 6 h. Scale bar: 50 μm.

encapsulation of ZIF-90 has little effect on the activity of Cyt c. After exposure to an elevated temperature of 90 °C for 150 min, the Cyt c encapsulated in ZIF-90 maintains 95% of its original activity, while free Cyt c is deactivated with only 65% of activity reserved. This phenomenon demonstrates that the structural confinement within ZIF-90 can protect the protein conformation of Cyt c [23]. In addition, after incubated with protease for 2 h, the ZIF-90 encapsulated Cyt c retains 91% of activity, which is decreased to 24% for free Cyt c. Thus, ZIF-90 can size-exclude the protease and prevent the proteolytic agents from contacting the embedded proteins. Consequently, UCMOFs can protect the protein drugs from the denaturation conditions and enhance the protein therapeutic efficacy.

The targeting ability of aptamers is investigated by incubating HeLa cells with sgc8-tethered UCMOFs for 6 h. The confocal laser scanning microscopy (CLSM) images show that the HeLa cells reveal a brighter UCL than that of the normal L02 cells (Fig. S12A in Supporting information). Further, HeLa cells are pre-treated with free sgc8 to block PTK7 receptors or treated with random DNA-tethered UCMOFs, which result in significantly reduced UCL signals as expected. Moreover, the internalization pathway is examined by colocalized characterization at subcellular level in a single HeLa cell. The spatial separation of UCL from endo/lysosome green fluorescence demonstrates that the UCMOFs are able to escape from endo/lysosome into cytosol after 6 h of incubation, where the drugs are released triggered by ATP (Fig. S12B in Supporting information).

The release of DOX from UCMOFs is investigated by incubating the sgc8-tethered UCMOF@DOX with HeLa cells for different time periods (Fig. 3A). The fluorescence of DOX shows a time-course enhancement, which is finally detected in nucleus, demonstrating the efficient delivery and intracellular release of DOX. The flow cytometric quantification also reveals the time-dependence of DOX uptake in HeLa cells (Fig. S13 in Supporting information). In addition, the HeLa cells show a weak UCL signal after incubation for 1 h, due to the insufficient cellular uptake and luminescence quenching by ZIF-90. When the reaction time reaches 6 h, a strong UCL signal is observed since more and more UCMOFs are internalized into cells with time, and the UCL is recovered owing to the ATP-induced decomposition of ZIF-90. Thus, the enhanced UCL can be used to monitor the release of drugs.

The delivery of therapeutic protein Cyt c is investigated by labeling Cyt c with FITC and encapsulating FITC-Cyt c into UCMOFs (Fig. 3B). The UCMOF@Cyt c-treated HeLa cells reveal a brighter FITC fluorescence than the free Cyt c-treated ones, indicating the efficient delivery of Cyt c by UCMOFs. The co-release of therapeutic agents from UCMOFs is also imaged by CLSM (Fig. 3C). After incubation for 6 h, FITC-Cyt c and DOX are observed in the cytosol and the nucleus respectively, further confirming the co-delivery and ATP-responsive release of multi-drugs *via* UCMOFs in cancer cells.

It is known that Zn^{2+} ions can induce the apoptosis through the generation of intracellular destructive ROS *via* a p53 pathway [19]. The dissociation of ZIF-90 shell into Zn^{2+} ions is confirmed by Zn^{2+} fluorescent probe, zinquin ethyl ester (Fig. S14 in Supporting information). Compared with the non-treated HeLa cells (control), the UCMOFs-treated HeLa cells reveal an enhanced blue fluorescence, which is similar to that of $Zn(NO_3)_2$-treated HeLa cells, suggesting the increased Zn^{2+} concentration due to the dissociation of ZIF-90 shell. In addition, the ability of UCMOFs to generate ROS in HeLa cells is monitored by a fluorescent probe, 2,7-dichlorofluorescein-diacetate (DCFH-DA), which can be deacetylated by cellular esterase and further oxidized by ROS to emit bright green fluorescence. Compared to UCNP@SiO_2, UCMOFs-treated HeLa cells reveal stronger green fluorescence of ROS specific probe (Fig. 4A). It has been confirmed that the ligands of ZIF-90 (ICA) cannot lead to the generation of ROS (Fig. S15 in Supporting information). Thus, intracellular ROS is induced by Zn^{2+}.

To investigate Cyt c-induced apoptosis pathway, the intracellular Cyt c and active caspase 3 are examined by Western blotting (Fig. 4B). The UCMOF@Cyt c-treated HeLa cells display a higher intensity of Cyt c immuno-detected protein band than the DMEM-treated cells or the free Cyt c-treated cells, which indicates the efficient protein delivery *via* the fabricated UCMOFs. In addition, the ratio of active caspase 3 to caspase 3 is increased with the increasing intracellular Cyt c, suggesting that Cyt c can induce the programmed cell death by activating the caspase-mediated apoptotic pathway.

Finally, the combinational therapy efficacy of sgc8-tethered UCMOF@DOX/Cyt c against HeLa cells is studied by MTT method. The nanovehicles with different formulations demonstrate a dose dependent cytotoxicity (Fig. 4C). The UCMOFs show a slight therapeutic performance with the cell viability more than 75%, which is only induced by the Zn^{2+}-mediated ROS production. When the UCMOFs encapsulate Cyt c or DOX, more than 70% cell growth inhibition is obtained at the administration concentration of 90 μg/mL, indicating the therapeutic efficacy of Cyt c or DOX in protein therapeutics or chemotherapy, respectively. In contrast, the free Cyt c shows a negligible cytotoxicity owing to its poor membrane permeability (Fig. S16 in Supporting information), which is consistent

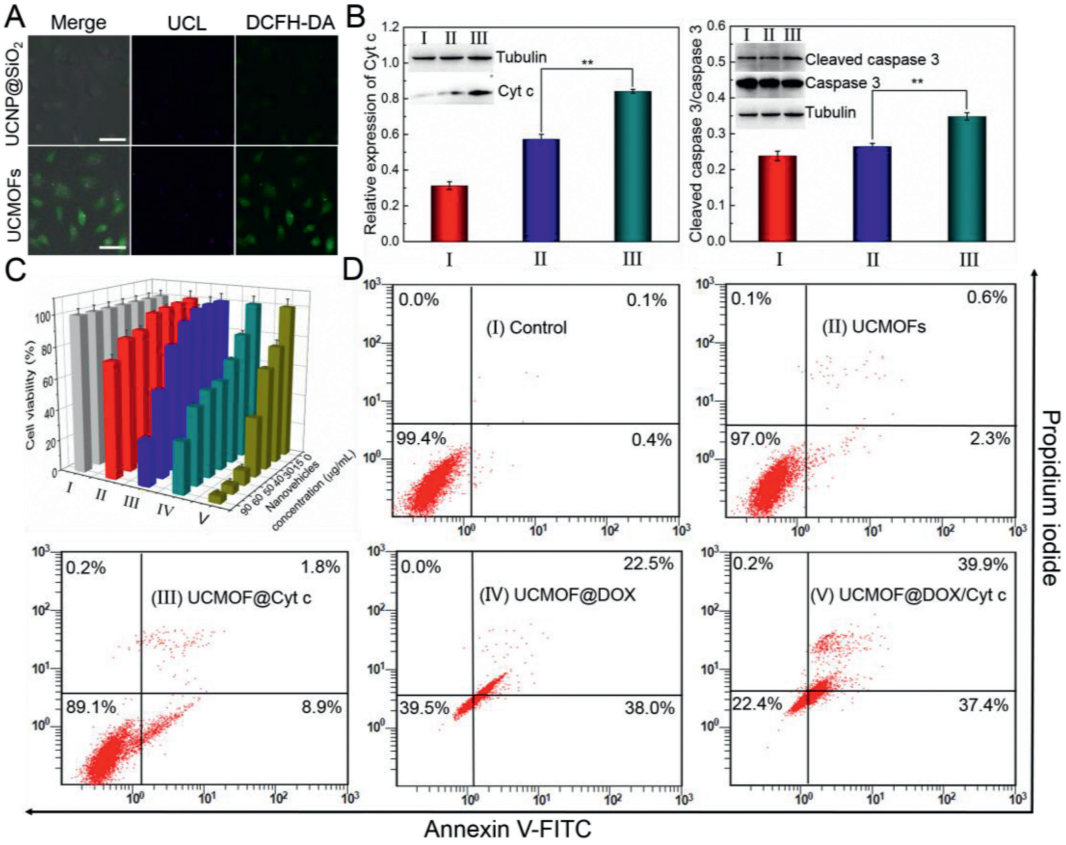

Fig. 4. (A) CLSM images of ROS in HeLa cells treated with UCNP@SiO_2 and UCMOFs, respectively. Scale bar: 50 μm. (B) Western blot analysis of expression of Cyt c and active caspase 3 in HeLa cells treated with (I) cell culture medium DMEM (control), (II) free Cyt c, and (III) sgc8-tethered UCMOF@Cyt c. $^{**}P < 0.01$ *vs.* free Cyt c (Two-tailed Student's *t*-test). Inset of B: Corresponding Western blotting images. (C) Cell viabilities and (D) flow cytometric analysis of HeLa cells treated with (I) cell culture medium DMEM (control), (II) sgc8-tethered UCMOFs, (III) sgc8-tethered UCMOF@Cyt c, (IV) sgc8-tethered UCMOF@DOX, and (V) sgc8-tethered UCMOF@DOX/Cyt c. Error bars represent the standard deviations from three independent measurements.

with the result of Western blot analysis. Notably, UCMOF@DOX/Cyt c exhibits more than 80% growth inhibition for HeLa cells at a lower administration concentration (50 μg/mL), indicating the promoted therapeutic performance of the combinational therapy.

The combinational treatment efficacy of the fabricated UCMOF@DOX/Cyt c is further investigated by flow cytometry (Fig. 4D). Compared to the cell culture medium-treated HeLa cells, the total apoptotic ratio of UCMOFs-treated cells increases to 3%, demonstrating the cytotoxicity of ROS produced by Zn^{2+}. The apoptosis is increased by 7.9% or 57.5% for Cyt c or DOX-encapsulated UCMOFs respectively, indicating that the drug-loaded UCMOFs can induce tumor cells into more severe apoptosis than the UCMOFs alone. As expected, the UCMOF@DOX/Cyt c acquires the highest apoptotic ratio of 77.5%, which is consistent with the results of MTT assays. These results are also verified by live/dead cell staining assays (Fig. S17 in Supporting information).

In summary, the ATP-responsive UCMOFs have been aqueous-phase synthesized for simultaneous transport of Cyt c (protein therapeutics), DOX (chemotherapy) and Zn^{2+} (generation of ROS for oxidative stress), achieving targeted combinational therapy of cervical cancer *via* specific recognition of aptamers. The UCL of UCMOFs can be effectively quenched by ZIF-90 shell and restored in response to intracellular ATP, which thus facilitates the real-time monitoring the release of therapeutic agents. Overall, as a robust and versatile multi-drugs delivery nanostructure, the fabricated stimuli-responsive UCMOFs open a new avenue for the development of nanoplatforms for targeted combinational cancer therapy along with *in situ* UCL imaging, which holds great promise in biomedical and clinical applications.

Declaration of competing interest

The authors declare that they have no known competing financial interests or personal relationships that could have appeared to influence the work reported in this paper.

Acknowledgments

We appreciate the support from the National Natural Science Foundation of China (Nos. 21834004 and 22076087), the Special Funds of the Taishan Scholar Program of Shandong Province (No. tsqn20161028), the Natural Science Outstanding Youth Fund of Shandong Province (No. ZR2020JQ08), the Youth Innovation Technology Program of Shandong Province (No. 2019KJC029), and the Program B for Outstanding PhD Candidate of Nanjing University (No. 201902B069).

Supplementary materials

Supplementary material associated with this article can be found, in the online version, at doi:10.1016/j.cclet.2021.07.007.

References

[1] X. Xu, W. Ho, X. Zhang, N. Bertrand, O. Farokhzad, Trends Mol. Med. 21 (2015) 223–232.
[2] Y. Li, X. Gao, Z. Yu, et al., ACS Appl. Mater. Interfaces 10 (2018) 15461–15466.
[3] M. Yu, J. Wu, J. Shi, O.C. Farokhzad, J. Control. Release 240 (2016) 24–37.
[4] B. Leader, Q.J. Baca, D.E. Golan, Nat. Rev. Drug Discovery 7 (2008) 21–39.
[5] S. Yue, X. Song, W. Song, S. Bi, Chem. Sci. 10 (2019) 1651–1658.
[6] K. Yu, Z. Qiao, W. Song, S. Bi, J. Anal. Test. 5 (2021) 112–129.

[7] S. Yue, Y. Li, Z. Qiao, W. Song, S. Bi, Trends. Biotechnol. 39 (2021) 1160–1172.
[8] X. Fu, G. Zhang, Y. Zhang, H. Sun, et al., Chin. Chem. Lett. 32 (2021) 1559–1562.
[9] X. Yang, Q. Tang, Y. Jiang, et al., J. Am. Chem. Soc. 141 (2019) 3782–3786.
[10] F. Lyu, Y. Zhang, R.N. Zare, J. Ge, Z. Liu, Nano Lett. 14 (2014) 5761–5765.
[11] F.K. Shieh, S.C. Wang, C.I. Yen, et al., J. Am. Chem. Soc. 137 (2015) 4276–4279.
[12] F.S. Liao, W.S. Lo, Y.S. Hsu, et al., J. Am. Chem. Soc. 139 (2017) 6530–6533.
[13] Y. Li, T. Gong, H. Gao, et al., Angew. Chem. Int. Ed. 60 (2021) 15472–15481.
[14] W.B. Liang, H.S. Xu, F. Carraro, et al., J. Am. Chem. Soc. 141 (2019) 2348–2355.
[15] H. Dong, S.R. Du, X.Y. Zheng, et al., Chem. Rev. 115 (2015) 10725–10815.
[16] L. Shen, T. Zhou, Y. Fan, et al., Chin. Chem. Lett. 31 (2020) 1709–1716.
[17] Y. Shao, B. Liu, Z. Di, et al., J. Am. Chem. Soc. 142 (2020) 3939–3946.
[18] Y. Liu, Y. Yang, Y. Sun, et al., J. Am. Chem. Soc. 141 (2019) 7407–7413.
[19] J. Wang, H. Wang, H. Wang, et al., ACS Nano 13 (2019) 5852–5863.
[20] F. Zheng, C. Wang, T. Meng, et al., ACS Nano 13 (2019) 12577–12590.
[21] Y. Pei, M. Li, Y. Hou, et al., Nanoscale 10 (2018) 11418–11429.
[22] F. Lu, L. Yang, Y. Ding, J.J. Zhu, Adv. Funct. Mater. 26 (2016) 4778–4785.
[23] G. Chen, S. Huang, X. Kou, et al., Angew. Chem. Int. Ed. 58 (2019) 1463–1467.